Journal of Visualization, Vol. 6, No. 4 (2003) 329-336

Three-dimensional Visualization of Diffusion Flame Shapes under Acoustic Excitation Using Stereoscopic Imaging and Reconstruction Technique

Ng, W. B.*[1], Salem, A. F. *[2] and Zhang, Y.*[2]

*1 Mechanical, Aerospace and Manufacturing Engineering Department, PO Box 88, University of Manchester Institute of Science and Technology, Manchester M60 1QD, United Kingdom.
E-mail: wen.ng@umist.ac.uk
*2 Mechanical, Aerospace and Manufacturing Engineering Department, PO Box 88, University of Manchester Institute of Science and Technology, Manchester M60 1QD, United Kingdom.
E-mail: yz100@umist.ac.uk

Received 29 March 2003
Revised 9 July 2003

Abstract : Stereoscopic imaging and reconstruction technique is introduced to reconstruct the flame structures that are subject to acoustic excitation. The laminar diffusion flame under investigation was created in a cylindrical tube and excited by a loudspeaker. Stereo images were taken at a shutter speed of 1/10000th second using a 'stereo camera' and the depth cue of the flame structures along the camera viewing direction were then computed using machine vision methodology. By visualizing the computed three-dimensional flame models, as well as judging the corresponding attribute such as surface gradient, the understanding of the flame and acoustic wave interaction could be improved.

Keywords : Three-dimensional Visualization, Acoustic Excitation, Laminar Diffusion Flame, Stereoscopic Imaging.

1. Introduction

Laminar diffusion flames under acoustic excitation could give rise to very complex flame patterns (Papadopoulos, et al., 2001). It is obvious that the resulting flame shape is a direct consequence of acoustic excitation, which either induced complex three-dimensional flow or acoustic pressure fluctuation. Therefore three-dimensional information of the flame geometry is useful in understanding the interaction of flame dynamics and acoustic excitations. Various optical diagnostic techniques have been employed to visualize an acoustic-excited flame for many decades. For examples, according to Putnam (1964), Mallard and Le Chatelier conducted one of the earliest photographic experiments of flames in an open-closed end tube in 1883. Thereafter, Markstein (1953) obtained the high-speed motion pictures of vibratory methane-air flame structures propagated in a tube by shadowgraphy technique. In recent years, Saito, et al. (1998) used CCD cameras with a motor drive to capture the behavior of an acoustic oscillated flame. Albers and Agrawal (1999) used rainbow Schlieren deflectometry (RSD) to investigate the structure of gas-jet diffusion flame in a tube. The reviewed optical techniques are not able to resolve the loss of in depth information, especially the detailed surface topology of flame structures in 3D. In this study an

innovative approach based on the combination of stereoscopic imaging and computer vision (Ng and Zhang, 2003a, 2003b) is applied to demonstrate the 3D structures of confined and acoustically excited laminar diffusion flame.

2. Stereoscopic imaging and flame structure reconstruction

The stereoscopic methodology used in this work, namely stereoscopic imaging and reconstruction, requires two slightly different perspective viewpoints of a scene so that the actual depth cue of the scene can be recovered. A stereo adapter is introduced to transform a digital camera into a 'stereo-camera' so that two views can be captured by a single chip of charge coupled device (CCD). The stereo-camera terminology is adhered to throughout this paper. As a result, only one camera is required to acquire a pair of stereo images and a typical example of it is shown in Fig. 2. It is worth mentioning that to the authors' knowledge, no one in the combustion community has ever utilized the stereo adapter for combustion and flame studies.

The proposed stereoscopic methodology basically can be further divided into two categories: they are optical stereoscopic imaging and digital stereoscopic reconstruction (Ng and Zhang, 2003a,b). The former is based on brainpower, which is still the most powerful 'computing machine' in many aspects of image processing and perception. However human brain is inadequate in resolving the physical dimension quantitatively. Computer vision, on the other hand, would excel in this area. The details of digital stereoscopic reconstruction are beyond the scope of this short paper and the readers are directed to the corresponding references. Nevertheless, its general concept is briefly described here. The technique is able to extract the actual depth cue and define the exact three-dimensional spatial location of flame shapes by means of computer vision computation (Faugeras, 1993). The steps for digital stereoscopic reconstruction include camera calibration (Tsai, 1987), correspondence problem (Zhang, 1995) and disparity computation (Alvarez, et al., 2002). The end result of this method gives a cloud of three-dimensional data containing spatial coordinates (x, y) and the depth magnitude (z) along the pixel grid. To help digest the obtained data set, parameterization has to be applied. It can be regarded as the numerical description of continuous geometrical surface. Considering each three-by-three subsurface, the z_i, is the depth value, the x_i and the y_i are the axes of node n_i in horizontal and vertical plane respectively, where $i = 1, 2, 3 \ldots 9$. The general equation of the surface can then be written as (Wood, 1996)

$$z = ax^2 + by^2 + cxy + dx + ey + f \tag{1}$$

The coefficients in Eqn. (1) are worked out as follow:

$a=(z_1+z_3+z_4+z_6+z_7+z_9)/6\delta^2-(z_2+z_5+z_8)/3\delta^2$,
$b=(z_1+z_2+z_3+z_7+z_8+z_9)/6\delta^2-(z_4+z_5+z_6)/3\delta^2$,
$c=(z_3+z_7-z_1-z_9)/4\delta^2$,
$d=(z_3+z_6+z_9-z_1-z_4-z_7)/6\delta$,
$e=(z_1+z_2+z_3-z_7-z_8-z_9)/6\delta$,
$f=(2(z_2+z_4+z_6+z_8)-(z_1+z_3+z_7+z_9)+5z_5)/9$, where δ is the pixel spacing in millimeter.

Slope is an important parameter to describe any three-dimensional continuous surface thoroughly. It is the rate of change of depth in both the x and y directions which can be used to identify the direction (aspect) and magnitude (gradient) of the steepest surfaces. So that surfaces can be interpreted in a geometrical sense. Mathematically, gradient can be found by combining the x and y component partial derivatives,

$$slope(magnitude) = \arctan\left(\frac{dz}{dxy}\right) = \arctan\left\{\sqrt{\left(\frac{\partial z}{\partial x}\right)^2 + \left(\frac{\partial z}{\partial y}\right)^2}\right\} \tag{2}$$

The slope magnitude of central pixel of each three-by-three subsurface can be calculated and so on. Each cell received a single integer value that indicates the magnitude of the deviation in degree.

3. Experimental apparatus and setup

3.1 Apparatus

A schematic diagram of the experimental apparatus is shown in Fig. 1. Basically, the rig consists of a burner, a cylindrical tube, a signal generating system and a stereoscopic imaging system.

The burner is a single copper fuel pipe of 0.005 m in inner diameter. There is an orifice at the end of the tube which reduces the overall inner diameter to 0.0018 m. The pipe is connected to a propane gas cylinder. The fuel is regulated by a control valve and measured by a rotameter, which has been calibrated with a dynamic range of 50 to 750 cm^3/min. The nozzle exit can be positioned at different height along the central axis of a cylindrical tube.

The cylindrical tube is made of thermoplastic material with a thickness of 0.3 cm. Its dimensions are 75.6 cm in height and 12.5 cm in inner diameter. It is supported by a thin sheet steel cowl of 37.8 cm in height. An optical window is created at the middle length of the tube for ease of optical access; a rectangular glass window with dimension of 7 cm (width) x 12 cm (height) x 0.2 cm (thickness) is held in place by aluminum ribs screwed on the side of the tube.

The signal generating system includes a signal generator (type J2B 10mW), an amplifier with impedance of 10Ω and a loudspeaker (BUMPER model). The amplitude of the supply voltage for the signal generator can be varied between 0 and 25 volts. The loudspeaker has a maximum power of 350 W and its frequency ranges from 25 Hz to 4000 Hz. Its effective diaphragm radius and area are 0.0875 m and 0.02405 m^2 respectively. Since the loudspeaker has a larger diameter than the thermoplastic tube, the cowl is used to connect the loudspeaker and the tube to ensure that as much of the sound as possible is transferred to the test section. The rear side of the speaker diaphragm is mounted on an enclosure (21 (width) x 21 (length) x 16 (height) cm) which is located at the bottom of the cowl. The enclosure projects some of the sound energy from the back of the loudspeaker that would otherwise have been lost.

The stereoscopic imaging system includes an Olympus E-100Rs digital camera and the stereo adapter. The adapter was mounted to the front filer ring of the digital camera and the image through the viewfinder is divided into left and right parts

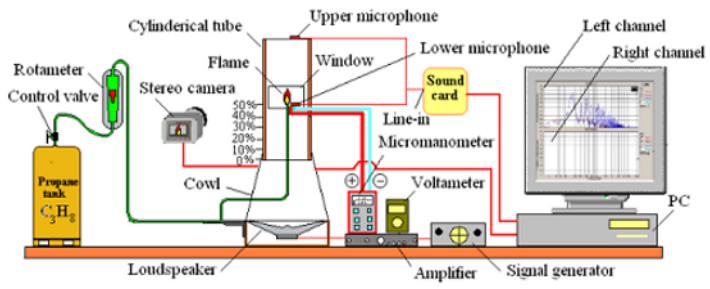

Fig. 1. Schematic diagram of the experimental setup.

3.2 Setup

In this experiment, the burner nozzle exit was positioned at the middle section of the tube and the stereo-camera was positioned at the right angle to the vertical tube axis. Without acoustic excitation, a laminar diffusion flame would form at the burner nozzle exit. The fuel flow rate was modulated at120 cm^3/min and the excitation frequency was 165 Hz. The voltage supply to the loudspeaker was varied from 0 to 16-volts at an interval of 2 volts. At each excitation level, fifteen pairs of stereo images were captured. Due to the high light intensity of the diffusion flame, the

maximum shutter speed of 1/10000th s was set for the image capturing process. Therefore flame time-scale down to 0.1 ms may be resolved. Considering the low Reynolds number in this experiment, the shutter speed is good enough in resolving the smallest wrinkling time scale of the flame. Camera calibration of the stereo apparatus has to be performed immediately after the image capturing process because the calibration has to be performed on the exact camera setup used to capture the images. The camera calibration approach of Zhang (2000) has been implemented in this application. It was carried out by capturing a 2D flat calibration grid, which contains a pattern of 8 x 8 squares, and for which the location of every corner of each square is known to a very high precision. Five images of the calibration grid at different orientations and positions were taken by the stereo-camera so that intrinsic parameters (Zhang, 2000, Ng and Zhang, 2003b) of the camera could be computed accordingly.

4. Results and Discussion

Figure 2 shows a typical pair of original stereo image taken by the stereo-camera. It can be seen that two images of different view perspective were captured on the same CCD chip. There is a rectangular black bar (vignette) at the center of the image, which is apparently caused by the plastic housing of the stereo adapter. Spatial resolution in the experiment was 0.163 mm/pixel. In this example, lower shutter speed was applied so that the burner nozzle and the background could be seen.

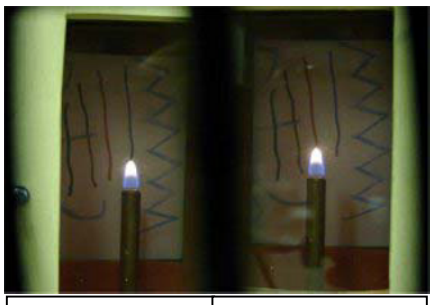

Fig. 2. A pair of stereo images of the unexcited laminar diffusion flame. Low shutter speed, 1/25th second, was used so that the background and the burner nozzle could be seen.

Figure 3 shows a sequence of the stereo images of the diffusion flame, which was excited at different amplitudes of the acoustic wave (by changing the supply voltage) but at the same excitation frequency (165Hz). The images on the left and right hand sides are extracted from the left and right image zones respectively. The gray square appeared in each image marks the position of burner nozzle exit. It is worth mentioning that at the leading edge of the surface of the yellow luminous region (stoichiometric mixture) there appears a thin blue layer, which is not able to be resolved at high shutter speed. As a result, the flames appear in the Fig. 3 (a-b) seem lifted off from the nozzle exit.

As we can see from Fig. 3 that without excitation (i.e. V=0), the flame had the appearance of an ordinary laminar flame. The length of the flame from its visible base to tip was invariant throughout. As amplitude increased, the flame length started to vary and oscillate dramatically, especially when the voltage supply was above 8 volts. At critical amplitude, the flame lifted off from the fuel nozzle. When the amplitude was further increased up to 20 volts (the corresponding images are not presented here) the whole flame texture changed from the yellow color of soot radiation to a clear blue flame and then the flame blew out. This phenomenon could be explained as follow: when

the supplied voltage to the loudspeaker (proportional to the amplitude of pressure wave) is increased, the laminar flame increases its height until turbulent mixing occurs. The flame length falls again and then lifts off with further increase of the pressure amplitude. This is attributed to the enhanced entrainment of the air at the burner rim (see Fig. 4). The flame color changed from yellow to blue is an indication of the enhanced mixing. Further increase of the amplitude, the flame becomes much more distorted. Pockets of burning gas were observed break away and eventually the flame were blown out.

V = 0 Volt

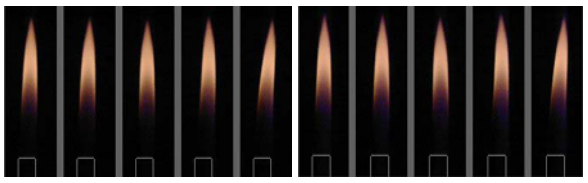

(a) Left image zone (b) Right image zone

V= 4 Volt

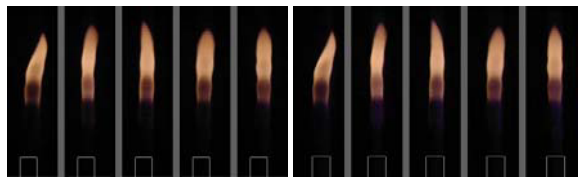

(c) Left image zone (d) Right image zone

V = 8 Volt

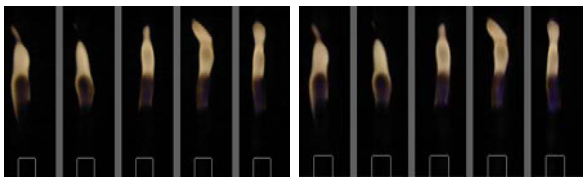

(e) Left image zone (f) Right image zone

V = 10 Volt

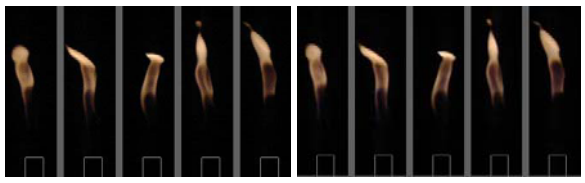

(g) Left image zone (h) Right image zone

V = 12 Volt

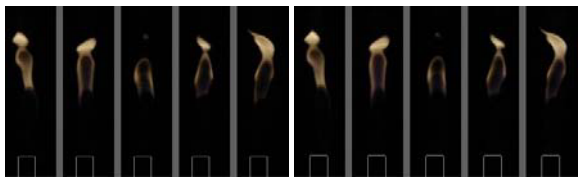

(i) Left image zone (j) Right image zone

V = 14 Volt

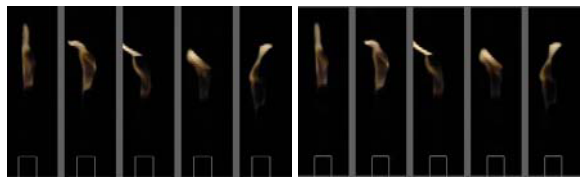

(k) Left image zone (l) Right image zone

Fig. 3(a)~(l). Flame dynamics in sequence excited by different supply voltage to the loudspeaker (f = 165 Hz, Total time record = 0.3333 second)

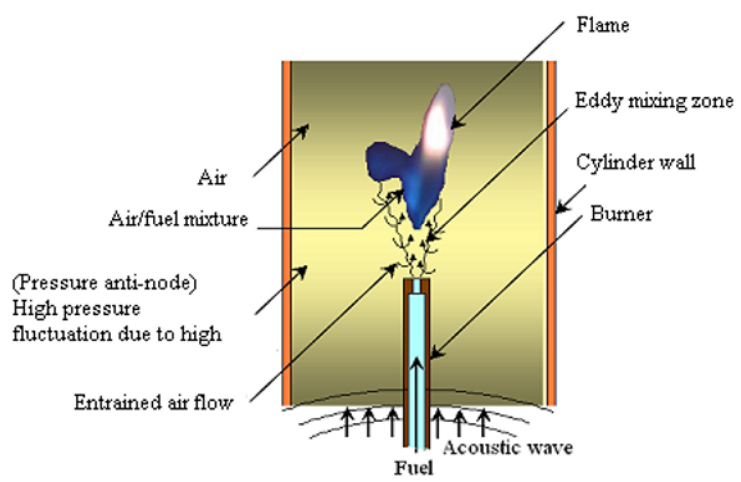

Fig. 4. Flame dynamics in sequence excited by different supply voltage to the loudspeaker.

Similar phenomenon would appear if an unconfined diffusion flame subjected to an excitation (Hertzberg, 1997). Saito, et al. (1998) reported that such a phenomenon may be useful for the control of soot production or product species. Note that the images above can only convey two-dimensional information such as flame height and width, whereas three-dimensional flame structure could provide detailed surface topology and improve the understanding of acoustic excitation effect on flame.

For illustration purpose, the first three pairs of the consecutive images in Fig. 3 (g)~(h) are used to demonstrate the stereoscopic methodology. Prior to reconstruction, it is found that the flame boundaries in each original stereo image are fairly distinctive from the background, except that the region just above the nozzle exit which has lower contrast and the intensity transition to the background is smooth. Therefore, a threshold of 40 pixel intensity was applied to isolate the flame front from the scene for ease of reconstruction. Figure 5 shows the sequence of snapshots of the reconstructed flame surfaces with texture mapped, which rotate about the vertical axes either in clockwise or anti-clockwise directions. This perspective effect delivers the realism of the three-dimensional flame surfaces.

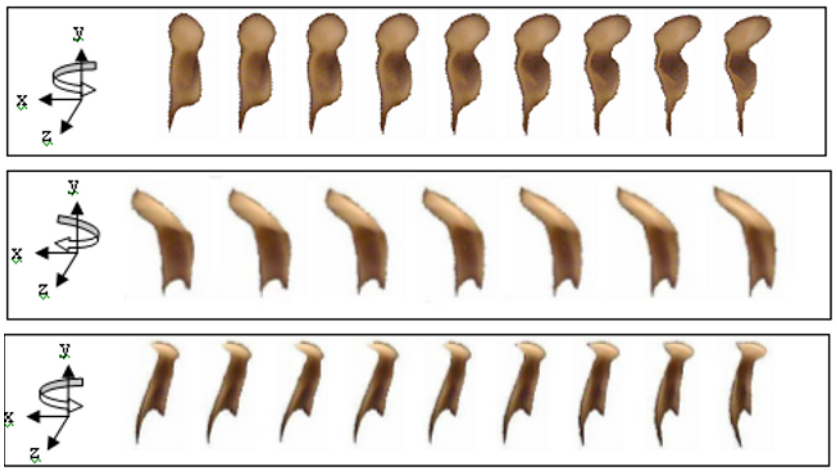

Fig. 5. The snapshots depict the realism of the selected reconstructed three-dimensional flame models from the flame patterns shown in Fig. 3(g)~(h).

Figure 6 depicts the surface gradient. The results vary from 0 (dark blue) to 90 (dark red) degree. The greater is the gradient; the steeper is the flame surface. From the figure, it is very obvious that the gradient is inhomogeneous and substantial throughout the flame surface, which indicates that the flame was considerably distorted and wrinkled when the forcing amplitude was high. It is worth mentioning that these surface 'wrinkles' are not observable by direct visualization.

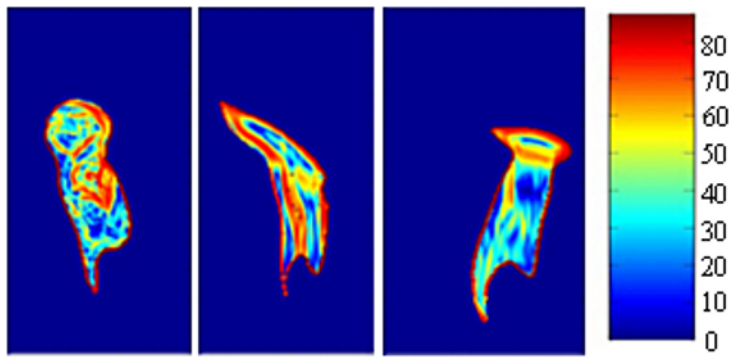

Fig. 6. Computed surface gradients of two flame patterns shown in Fig. 3(h)~(g).

Apart from gradient computation, flame topology is also presented in 3D space as seen in Fig. 7. In the plots the color legend references the depth of flame surface topology and the more reddish is the color, the further away it is from the viewer. The coordinates indicate the approximate physical size of the flame in centimeter unit. Such information is necessary to reveal the real topology of the flame, from which data such as surface to volume ratios and curvature can be calculated. From Figs. 6 and 7, it can be seen that the jet flame under acoustic excitation are highly wrinkled and irregular. All reconstructed flame structures in Fig. 7 are superimposed into a single 3D plot (see Fig. 8) in order to exam the extent of flame changes caused by acoustic excitation. It seems that the flame tip is more sensitive to the excitation. The 3D movement of the flame implies that the local flow within the cylinder is highly three dimensional despite the fact that the acoustic pressure wave inside the cylinder is essentially 1D. Further investigation in this aspect is worthwhile.

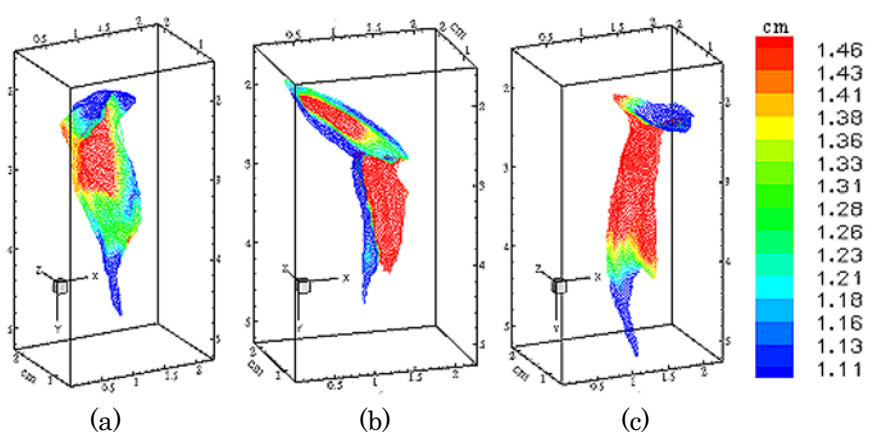

Fig. 7(a)~(c). Reconstructed flame models of flame patterns shown in Fig. 3(g)~(h) in three-dimensional space. Multi-color scale is used to reference the depth cue.

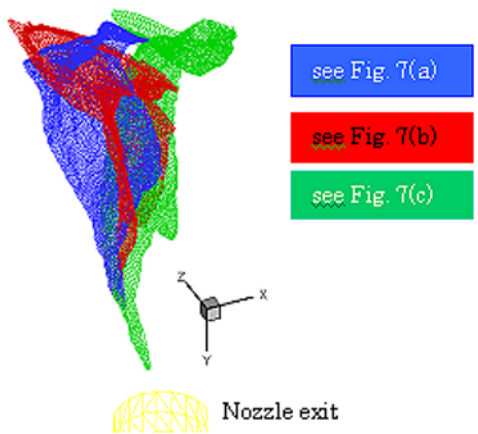

Fig. 8. Superimposition view of the reconstructed flame shapes shown in Fig. 7.

It is worth noting that since it is difficult to predict the accuracy through the geometric measurement of constructed flame models due to the flame's inherent phenomena. The accuracy of the 3D reconstruction was verified with a known particle movement in 3D. The particle movement is arranged in such a way that the 3D coordinate of the particle could be calculated trigonometrically. Then 3D stereo imaging and reconstruction were performed. The reconstructed results were then compared with the corresponding calculated value. The error is 8% (Ng and Zhang, 2003b).

5. Conclusion

Stereoscopic imaging and reconstruction have been applied to visualize and study the dynamics of flame under acoustic excitation. Three-dimensional view of the excited flame shape has been constructed via stereo computer vision. Surface gradient and curvature are calculated to quantify the characteristics of the flame surfaces of interest. It is able to reveal flame structures that are not observable by direct visualization. The potential of the proposed methodology for the study of flame dynamics has been demonstrated.

References

Albers, B. W. and Agrawal, A. K., Schlieren Analysis of an Oscillating Gas-Jet Diffusion Flame, J. of Combustion and Flame, 119 (1999), 84.

Alvarez, L., Deriche, R., Sánchez, J. and Weickert, J., Dense Disparity Map Estimation Respecting Image Discontinuities: A PDE and ScaleSspace Based Approach, J. of Visual Communication and Image Representation 13 (2002), 3.

Faugeras, O., Three-Dimensional Computer Vision: A Geometric Viewpoint, Cambridge: MIT Press (1993).

Hertzberg, J. R., Conditions for a Split Diffusion Flame, Combustion and Flame, 109 (1997), 314.

Markstein, G. H., Instability Phenomena in Combustion Wave, Fourth Symposium International on Combustion, 44 (1953).

Ng, W. B., and Zhang, Y., Stereoscopic Imaging and Reconstruction of the 3D Geometry of Flame Surface, Experiments in Fluids, 34 (2003), 484.

Ng, W. B., and Zhang, Y., Stereoscopic visualization and Reconstruction of Turbulence Flames, IS&T/SPIE International Symposium on Electronic Imaging: Science and Technology, Santa Clara, USA (2003).

Papadopoulos, T., Pritchard, M., Green, C. and Zhang, Y., Flame Patterns of Acoustic Wave and Flame Interaction in a Cylindrical Tube, J. of Visualization, 4-2 (2001), 179.

Putnam, A. A. and Chapter G. Experimental and Theoretical Studies of Combustion Oscillations. Non-Steady Flame Propagation. G. H. Markstein. New York, Pergamon Press Ltd. (1964).

Saito, M., Sato, M. and Nishimura, A., Soot Suppression by Acoustic Oscillated Combustion, The Fuel, 77-9 (1998), 973.

Tsai, R. Y., A Versatile Camera Calibration Technique for High-Accuracy Three-Dimensional Machine Vision Metrology using off-the-shelf TV Cameras and Lenses, J. of Robotics and Automation IEEE., RA-3 (1987), 323.

Wood, J., The Geomorphological Characterisation of Digital Elevation Models, Ph.D. thesis, Univ. of Leicester, UK (1996).

Zhang, Z. Y., A Robust Technique for Matching Two Uncalibrated Images through the Recovery of the Unknown Epipolar Geometry, Artificial Intelligence, 78 (1995), 87.

Zhang, Z. Y., A Flexible new Technique for Camera Calibration, IEEE Trans Pattern Analysis Machine Intelligent, 22 (2002), 1330.

Author Profile

Wen B. Ng: He received his 1st class BEng degree in Mechanical Engineering from UMIST in 1999. Currently, he is at his Ph.D. writing-up stage in the same university. He is partly sponsored by ALSTOM POWER, Rolls-Royce Plc, British Government and UMIST. His research is mainly focused on stereoscopic methodology of flame dynamics and combustion instability study in gas turbine combustor.

Salem A. Farhat: He received his BSc degree in Mechanical Engineering from Al-Fateh University in Libya (1986). After that, he received M.Sc. degree from Warsaw University in Poland (1996) in the field of Mechanical Engineering and became a lecturer in Al-Fateh University until 2000. Currently, he is studying in UMIST for a Ph.D. degree in the area of combustion instability.

Yang Zhang: He received his B.Eng. degree in Cryogenic Engineering from Zhejiang University, China and his Ph.D. in combustion from Cambridge University, England. He worked in No. 585 Research Institute, China, and studied English in Shanghai Foreign Language Institute before starting his Ph.D., which was in the area of experimental combustion and under the supervision of Prof. K N C Bray, FRS. After his Ph.D. he continued his research in Cambridge University before taking up his current position as a lecturer and then senior lecturer at UMIST. His research interests include the experimental and computational studies of reacting flows, experimental diagnostic techniques such as PIV, high-speed imaging, stereoscopic imaging and computing, signal processing and flame pattern recognition.